JACS
JOURNAL OF THE AMERICAN CHEMICAL SOCIETY
pubs.acs.org/JACS
Communication

Ordered Graphane Nanoribbons Synthesized via High-Pressure Diels–Alder Polymerization of 2,2′-Bipyrazine

Fang Li, Xingyu Tang, Yunfan Fei, Jie Zhang, Jie Liu, Puyi Lang, Guangwei Che, Zilin Zhao, Yuqing Zheng, Yuan Fang, Chen Li, Dexiang Gao, Xiao Dong, Takanori Hattori, Jun Abe, Ho-kwang Mao, Haiyan Zheng, and Kuo Li*

Cite This: J. Am. Chem. Soc. 2025, 147, 14054–14059
Read Online
ACCESS | Metrics & More | Article Recommendations | Supporting Information

ABSTRACT: Graphane shares the same two-dimensional honeycomb structure of graphene, but its saturated carbon skeleton gives rise to a bandgap and therefore provides more possibilities for the development of novel carbon-based semiconductors. However, the hydrogenation of graphene usually leads to disordered and incompletely hydrogenated graphane, and the precise synthesis of graphane with a specific configuration is still very challenging. Here, we synthesized a crystalline graphane nanoribbon (GANR) via pressure-induced polymerization of 2,2′-bipyrazine (BPZ). By performing Rietveld refinement of in situ neutron diffraction data, nuclear magnetic resonance spectroscopy, infrared spectra, and theoretical calculation, we found that BPZ experienced Diels–Alder polymerization between the $\pi\cdots\pi$ stacked aromatic rings and formed extended boat-GANR structures with exceptional long-range order. The unreacted −C═N− groups bridge the two ends of the boat and are ready for further functionalization. The GANR has a bandgap of 2.25 eV, with booming photoelectric response (I_{ON}/I_{OFF} = 18.8). Our work highlights that high-pressure topochemical polymerization is a promising method for the precise synthesis of graphane with specific structure and desired properties.

Graphane $(CH)_n$ is the H-saturated graphene and can be regarded as the thinnest two-dimensional (2D) diamond, which opens the bandgap of graphene,[1−6] like the well-known graphene nanoribbons.[7−9] This fully saturated 2D nature brings promising physical properties, like potential superconductivity with T_c up to ∼90 K (doped by B)[10] and excellent dielectric properties. By modifying the amount and the ordering of hydrogen, many materials, even 2D nanoelectronics, can be expected with desirable electronic and magnetic properties, like graphone, graphene "nanoroad", and graphane $p-n$ junctions.[11] However, most of the theoretical predictions neglected the isomerism of graphane and focused on the simplest model (graphane I, Scheme 1). Due to the various arrangement of C−H bonds above or below the plane, the hexagonal rings may adopt chair, boat, and twisted structures. Graphane therefore has many isomers, varying in the electronic, optical, and chemical properties.[1,12] For example, Graphane I is the most stable isomer.[1,13] Desorption of hydrogen from one side would yield a ferromagnetic semiconductor.[14] Graphane II is isoelectronic with the black-phosphorus nitrogen,[15] which is a promising substrate for the research of semiconductors. The vibrational spectrum of Graphane III varies significantly from Graphane I[1,16] and would affect the phonon–electron coupling and therefore the superconductivity. When substituted by F, −OH, or $-NH_2$ the stabilities of these isomers may change, increasing the complexity for synthesis.[17−19]

Scheme 1. Typical Graphane Isomers[a]

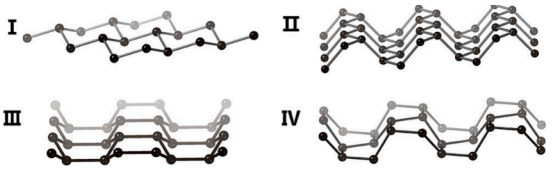

[a]H are omitted for clarity.

Many methods were used to synthesize graphane, like low-pressure H_2 plasma,[4,20] high-pressure H_2 hydration,[21] wet-chemistry Birch reactions,[22−24] and high-temperature–high-pressure synthesis from organics.[25] However, these methods are limited to the unsatisfied crystallinity and selectivity of product,[26] as it is hard to control the direction of hydrogen's attack.[4] Thus, the precise synthesis of highly ordered structure-specific graphane is urgently required.

Pressure-induced polymerization (PIP) has demonstrated its adaptability in the preparation of extended carbon structures like carbon nanothreads and nanoribbons, as well as graphane.[27−37] Acetylene transforms into nanometer-range ordered Graphane II via PIP.[36,38] The $C_6F_6-C_6H_6$ cocrystal transforms into F-orderly substituted nanometer-range ordered graphane III via Diels–Alder PIP, which highlighted that the PIP of substituted aromatics is an effective method to construct graphane with specific configurations.[37] In this work, we

Received: February 20, 2025
Revised: April 6, 2025
Accepted: April 16, 2025
Published: April 21, 2025

https://doi.org/10.1021/jacs.5c03116
J. Am. Chem. Soc. 2025, 147, 14054–14059

synthesized Graphane III nanoribbons (GANRs) with atom-scale ordering via the Diels–Alder PIP of 2,2′-bipyrazine (BPZ) at 20 GPa, which paved the way to the precise synthesis of desired graphane.

BPZ has a triclinic structure with one molecule per unit cell at ambient conditions (P-1, a = 3.76 Å, b = 5.35 Å, c = 9.52 Å, α = 102.96°, β = 91.98°, γ = 101.69°, Figure 1a and b).[39] The

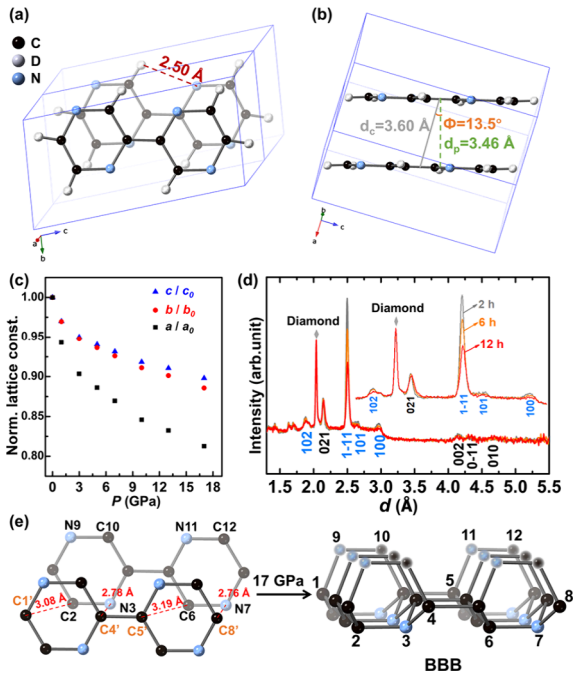

Figure 1. Crystallographic investigation of BPZ. Crystal structure of BPZ viewed (a) perpendicular to and (b) parallel to the molecular plane at ambient pressure. (c) Anisotropic compressibility of lattice parameters. (d) Time-dependent in situ neutron diffraction at 20 GPa. (e) Formation of BPZ-GANR (BBB).

two pyrazine rings in BPZ are coplanar due to the intramolecular N···H hydrogen bonds. The molecules are slip-stacked along the a-axis with slip angle Φ = 13.5°, much smaller than that of benzene[40] and aniline,[41] etc., and the perpendicular intermolecular distance is d_p = 3.46 Å. Meanwhile, the N atoms in BPZ increase the reactivity due to the decreased Pauli repulsion between the diene and the dienophile.[42,43] All of these characteristics suggest that BPZ is an excellent precursor to polymerize along the a-axis to generate crystalline product.

As indicated by in situ high-pressure Raman and infrared spectra (IR) experiments (Figures S1 and S2 and Table S1), BPZ polymerizes at ∼20 GPa at room temperature. Above 19.9 GPa, the Raman signals gradually disappear, and IR spectra show several new peaks at 915, 1308, and 1660 cm^{-1}, suggesting a chemical reaction. In situ neutron diffraction of deuterated BPZ shows that the compressibility of BPZ is highly anisotropic (Figures 1c and S3 and Table S2). Up to 17 GPa, the a-axis (π–π stacking direction) is compressed by 18.49%, much larger than that of the b-axis (11.06%) and c-axis (9.75%), suggesting higher reaction probability along the a-axis.[44,45] At 20 GPa, the hkl ($h \neq 0$, e.g., 100, 101, 1−11, and 102) peaks degraded significantly with time, indicating the atoms are moving out of the (100) plane and unambiguously demonstrating the bonding along the a-axis (Figure 1d).

The crystal structure of BPZ at threshold pressure (17 GPa) was determined by the Rietveld refinement and subsequent geometric optimization of atomic coordinates by density functional theory (DFT) calculation (Figures S3c and 1e and Table S3). The parallel $\pi\cdots\pi$ stacking of BPZ is maintained along the a-axis, with the closest intermolecular distance of 2.76 Å between C4′-N3 and C8′-N7. This already reached the critical reaction distance of the typical aromatics at room temperature, like $d_{C\cdots C}$ = 2.8 Å in benzene,[46] benzene-hexafluorobenzene (C_6H_6–C_6F_6) cocrystal,[37] and 2,5-furandicarboxylic acid,[33] as well as $d_{C\cdots N}$ = 2.9 Å for s-triazine,[32] and would lead to sequential Diels–Alder reactions along the a-axis (C=C−N=C and C=N as diene and dienophile, respectively, Figure 1e) and produce BPZ GANR. The product has the Graphane III skeleton with all the three newly produced cyclohexane rings in boat configuration, which is therefore referred to as BBB with the systematic nomenclature shown in Figure S4.

We then synthesized the product in milligram scale at 30 GPa using a VX3 Paris-Edinburgh press (PE30, details in SI), whose X-ray diffraction (XRD) peaks (Figure 2a) were consistent with the in situ neutron experiments (Figure S5). The diffractions indexed as $0kl$ (e.g., 001, 0−11, 010, 002, 0−12, and 011) were observed, which can be traced from the precursor. This is a distinctive feature of topochemical reactions, as reported in several similar PIP reactions.[31,32] The minimum observed d-spacing of PE30 was 1.8 Å, demonstrating atom-level ordering.

We performed Rietveld refinement using the BBB model. Since only the $0kl$ peaks are detectable, only the atomic coordinates on the b–c plane can be determined by a 2D-refinement. A unit cell with b = 5.58 Å, c = 10.08 Å, α = 120°, and $\beta = \gamma$ = 90° and space group P1 were selected; a was set to 0.33 Å to avoid any interference of hkl ($h \neq 0$) peaks. The resulting wR_p is 8.48%, which demonstrated the reliability of the BBB (Figure 2b). The high-resolution transmission electron microscope (HRTEM) image of PE30 also showed clear d-spacing of 10.0 Å (Figure 2c), consistent with the 001 peak in XRD. This is related to the width of the BPZ-GANR and demonstrates good stacking order (Figure S6).

The intraribbon structure of PE30 was studied by using IR (Figure 2d) and solid-state nuclear magnetic resonance spectroscopy (ssNMR, Figure 2f). C(sp^3)–H stretching at ∼2850, 2925, and 2955 cm^{-1} and C=N stretching at ∼1620 cm^{-1} were observed in the IR spectrum. The former demonstrates the bonding between the aromatic rings, and the latter indicates that part of the C=N groups is still unreacted, consistent with the simulated IR of the BBB.

The ^{13}C cross-polarization magic angle spinning (CP-MAS) ssNMR spectrum with contact time of 2000 μs was shown in Figure 2f (blue curve), in which both hydrogenated and nonhydrogenated carbon was detected. In the region of sp^2-C, the peak at 145 ppm is ascribed to the sp^2-C(=N), with its neighbor at ∼165 ppm attributed to the sp^2-C(=NH),[47−49] due to protonation by moisture (Figure S7). In the sp^3-C region, five peaks were observed at 54, 58, 68, 73, and 78 ppm, respectively. In a following short one-bond ^{1}H–^{13}C CP ssNMR spectrum (contact time 50 μs, orange curve), where only the hydrogenated C can be detected, the peaks at 73 and 78 ppm disappeared, indicating that they were quaternary carbons while others were the HCR_3 carbons.

To make a quantitative study, we collected the direct-polarization (DP) ^{13}C ssNMR spectrum (Figure 2f) and

https://doi.org/10.1021/jacs.5c03116
J. Am. Chem. Soc. 2025, 147, 14054−14059

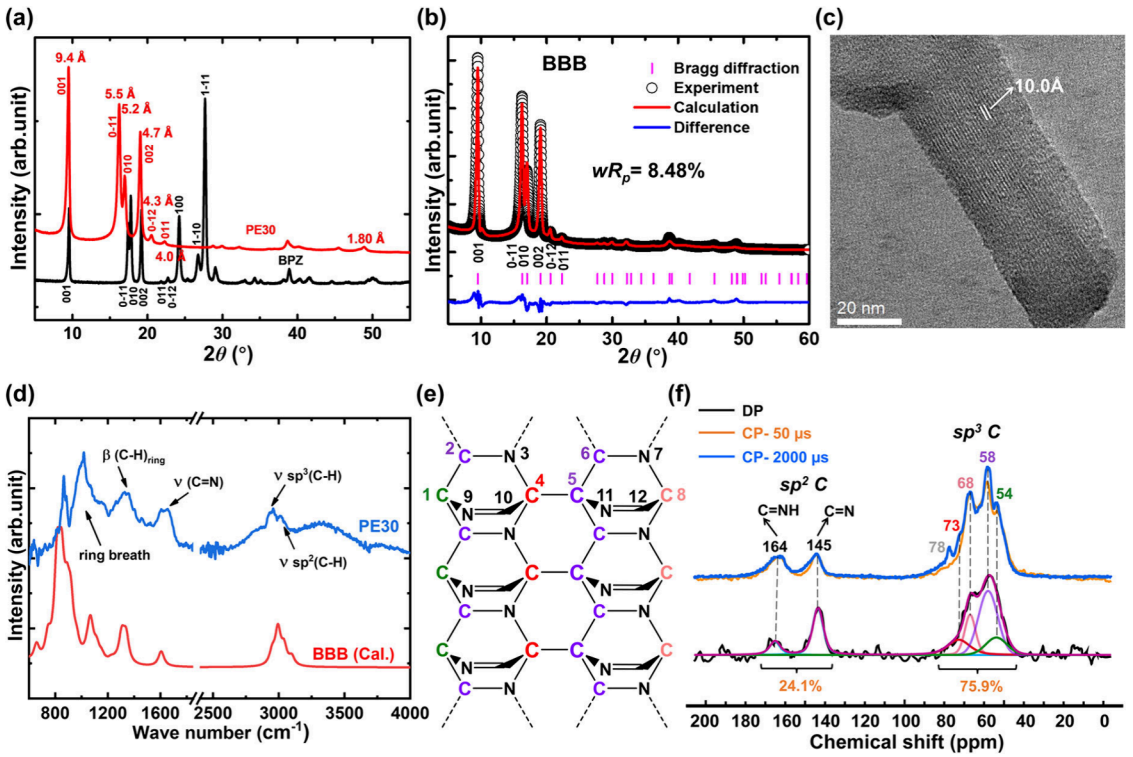

Figure 2. Structure of polymerized BPZ. (a) XRD pattern of PE30 (BPZ for comparison) and (b) Rietveld refinement plot using the BBB model. (c) HRTEM image of PE30. (d) Experimental (PE30) and calculated IR spectra (BBB) of the polymerized BPZ at ambient pressure. (e) The proposed structure of the BBB. (f) ^{13}C CP-MAS and DP ssNMR spectra of PE30. The blue and orange lines represent the signals with the contact time of 2000 and 50 μs, respectively. The deconvolution results of DP are colored following the labels in (e).

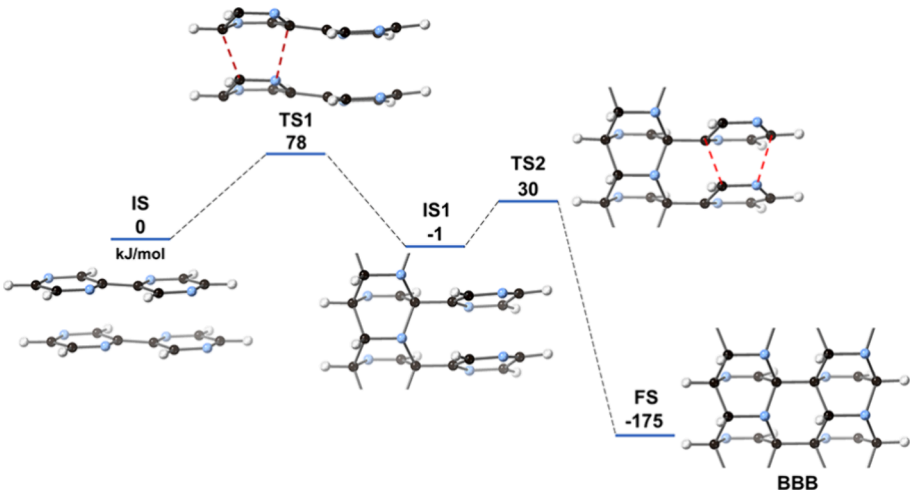

Figure 3. Theoretical investigation of the Diels–Alder reaction path from BPZ to BBB GANR at 20 GPa.

deconvoluted the peaks with their positions extracted from the CP. The ratio of integrated peak intensities of sp^2-C to sp^3-C is 24.1%:75.9% (1:3), consistent with the BBB model (Figures 1e and 2e). In the region of sp^3-C, four peaks were concluded corresponding to four kinds of carbons in the BBB model. The peak at 73 ppm is assigned to C4 due to the strong deshielding by the two N atoms and its quaternary carbon nature. The peak at 68 ppm is attributed to C8, which is also bonded to two N atoms but one H atom. The peaks at 58 and 54 ppm are contributed to C2/C6 and C1, which was bonded to one N atom, respectively, while C5 is also assigned to the peak at 58 ppm due to its indistinguishable chemical shift compared to C2/C6.[50] The peaks at 73, 68, 58, and 54 have a content ratio of 11.3:13.2:40.4:11, approximately 1:1:3:1, which is consistent with the carbon content ratio in the BBB and therefore perfectly confirms its structure. The peak at 78 ppm identified in the CP spectrum is neglected due to the weak intensity, probably attributed to the side product.

The reaction path from BPZ to BBB BPZ-GANR at 20 GPa was then evaluated by a theoretical calculation using the nudged elastic band (NEB) method. As shown in Figure 3, a two-step Diels–Alder reaction from BPZ (initial state, IS) to IS1 and from IS1 to BBB (final state, FS) was identified with energy barriers of 78 and 31 kJ/mol $C_8N_4H_6$, respectively. As the room-temperature reaction typically requires an energy barrier below 100 kJ/mol, this path is feasible. As discussed in

https://doi.org/10.1021/jacs.5c03116
J. Am. Chem. Soc. 2025, 147, 14054–14059

several theoretical studies, the involvement of N would decrease the Pauli repulsion and promote the reactivity of the arenes in the Diels–Alder reaction.[42,43]

The PIP of BPZ changes its optical properties. The BPZ crystal darkens significantly above 16.5 GPa (Figure S8), and the bandgap decreased correspondingly, as disclosed by the UV–vis spectrum (Figure S9). When decompressed to ambient pressure, the sample became brown with an optical bandgap of 2.25 eV (Figure 4a), much smaller than that of the

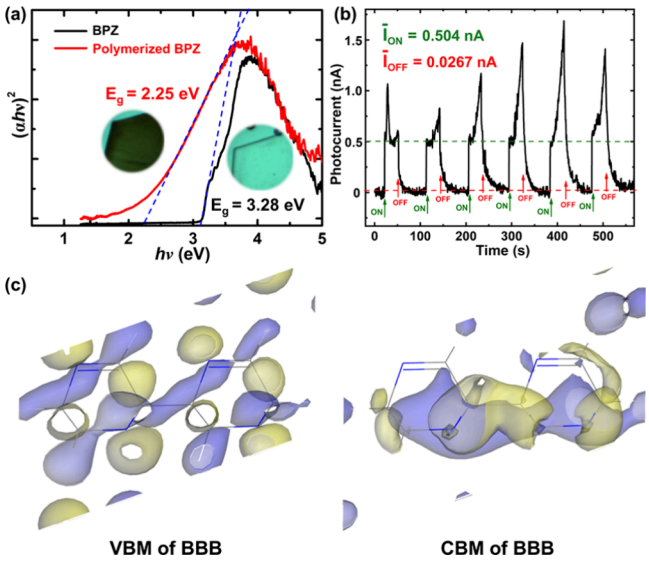

Figure 4. Optical properties of poly-BPZ. (a) Optical bandgap of BPZ and polymerized BPZ. (b) Photocurrent of PE30. (c) Distribution of VBM and CBM of the BBB.

predicted graphane (>3.5 eV)[1] due to the unreacted −C═N− and the N atoms in the graphane framework, like pyridine nanothreads.[51] PE30 shows a photoelectric response to visible light (Figures 4b and S10). When the light is turned on, the current increased from 0.0267 to 0.504 nA and recovered when off. The I_{ON}/I_{OFF} ratio is 18.8. The rise time (τ_r) is 0.38 s (Figure S11), suggesting a very quick response. This may promote fascinating applications of GANRs in modern electronics.[52]

The origin of the photocurrent was then examined by a theoretical calculation. The BBB exhibits its valence band maximum (VBM) and conduction band minimum (CBM) at the Γ-point. The VBM is mainly distributed on the unreacted −C═N−, whereas the CBM is mainly in the graphane framework (Figure 4c). Therefore, the free charge carrier may result from the electron transfer from −C═N− to the graphane framework.[53,54]

In summary, a highly ordered −C═N− bridged all-boat structure GANR was synthesized via the Diels–Alder polymerization of BPZ under 20 GPa. The remaining −C═N− groups modified the bandgap of the GANR, which shows an evident photocurrent response. Our work shows that the PIP of polyaromatics is a robust method to synthesize well-defined and functionalized graphane materials with specific configurations. The bandgap of the graphane can therefore be modified and has potential photoelectric applications. Based on this proof-of-concept work, more functional groups can be incorporated to modify the electronic structure of graphane and its electronic and photonic properties.

■ ASSOCIATED CONTENT

Supporting Information

The Supporting Information is available free of charge at https://pubs.acs.org/doi/10.1021/jacs.5c03116.

Experimental procedures: characterization methods of in situ high-pressure Raman, IR, UV–vis, and neutron diffraction experiments; the preparation of deuterated BPZ; synthetic method of PE30; characterization methods of PE30 by XRD, HRTEM, IR, and ssNMR experiments; optimization of crystal structures at the threshold pressure of reaction; construction of structural models BPZ-GANRs; calculation method of IR spectrum; and band structures of BPZ-GANRs (PDF)

■ AUTHOR INFORMATION

Corresponding Author

Kuo Li − *Center for High Pressure Science and Technology Advanced Research, Beijing 100193, People's Republic of China;* orcid.org/0000-0002-4859-6099; Email: likuo@hpstar.ac.cn

Authors

Fang Li − *Center for High Pressure Science and Technology Advanced Research, Beijing 100193, People's Republic of China*

Xingyu Tang − *Center for High Pressure Science and Technology Advanced Research, Beijing 100193, People's Republic of China*

Yunfan Fei − *Center for High Pressure Science and Technology Advanced Research, Beijing 100193, People's Republic of China*

Jie Zhang − *Center for High Pressure Science and Technology Advanced Research, Beijing 100193, People's Republic of China*

Jie Liu − *Center for High Pressure Science and Technology Advanced Research, Beijing 100193, People's Republic of China*

Puyi Lang − *Center for High Pressure Science and Technology Advanced Research, Beijing 100193, People's Republic of China*

Guangwei Che − *Center for High Pressure Science and Technology Advanced Research, Beijing 100193, People's Republic of China*

Zilin Zhao − *Center for High Pressure Science and Technology Advanced Research, Beijing 100193, People's Republic of China*

Yuqing Zheng − *Center for High Pressure Science and Technology Advanced Research, Beijing 100193, People's Republic of China*

Yuan Fang − *Center for High Pressure Science and Technology Advanced Research, Beijing 100193, People's Republic of China*

Chen Li − *Center for High Pressure Science and Technology Advanced Research, Beijing 100193, People's Republic of China;* orcid.org/0000-0002-1563-6939

Dexiang Gao − *Center for High Pressure Science and Technology Advanced Research, Beijing 100193, People's Republic of China;* Present Address: Institute of High Energy Physics, Chinese Academy of Sciences, 100049 Beijing, People's Republic of China; Spallation Neutron Source Science Center, Dongguan, Guangdong 523803, People's Republic of China

Xiao Dong − *Key Laboratory of Weak-Light Nonlinear Photonics, School of Physics, Nankai University, Tianjin 300071, People's Republic of China;* orcid.org/0000-0003-4533-1914

Takanori Hattori − *J-PARC Center, Japan Atomic Energy Agency, Ibaraki 319-1195, Japan*

Jun Abe − *Neutron Science and Technology Center, Comprehensive Research Organization for Science and Society, Ibaraki 319-1106, Japan*

Ho-kwang Mao − *Center for High Pressure Science and Technology Advanced Research, Beijing 100193, People's Republic of China*

Haiyan Zheng − *Center for High Pressure Science and Technology Advanced Research, Beijing 100193, People's Republic of China;* orcid.org/0000-0002-4727-5912

Complete contact information is available at: https://pubs.acs.org/10.1021/jacs.5c03116

Author Contributions

All authors have given approval to the final version of the manuscript.

Notes

The authors declare no competing financial interest.

■ ACKNOWLEDGMENTS

The authors acknowledge the support of the National Key Research and Development Program of China (2023YFA1406200). The authors also acknowledge the support of the National Natural Science Foundation of China (NSFC) (Grant no. 22022101). In situ high-pressure neutron diffraction experiment at the Materials and Life Science Experimental Facility of the J-PARC was performed through user programs (Proposal No. 2023B0030 and 2024A0054). This study was also partially supported by Synergetic Extreme Condition User Facility (SECUF).

■ REFERENCES

(1) Sofo, J. O.; Chaudhari, A. S.; Barber, G. D. Graphane: A Two-Dimensional Hydrocarbon. *Phys. Rev. B* **2007**, *75*, 153401.

(2) Boukhvalov, D. W.; Katsnelson, M. I.; Lichtenstein, A. I. Hydrogen on Graphene: Electronic Structure, Total Energy, Structural Distor-tions and Magnetism from First-Principles Calcu-lations. *Phys. Rev. B* **2008**, *77*, No. 035427.

(3) Jones, J. D.; Mahajan, K. K.; Williams, W. H.; Ecton, P. A.; Mo, Y.; Perez, J. M. Formation of Graphane and Partially Hydrogenated Graphene by Electron Irradiation of Adsorbates on Graphene. *Carbon* **2010**, *48*, 2335−2340.

(4) Elias, D. C.; Nair, R. R.; Mohiuddin, T. M. G.; Morozov, S. V.; Blake, P.; Halsall, M. P.; Ferrari, A. C.; Boukhvalov, D. W.; Katsnelson, M. I.; Geim, A. K.; Novoselov, K. S. Control of Graphene's Properties by Reversible Hydrogenation: Evidence for Graphane. *Science* **2009**, *323*, 610−613.

(5) Agbenyega, J. Graphane Hits the Stage: Carbon. *Mater. Today* **2009**, *12*, 13.

(6) Zhou, C.; Chen, S.; Lou, J.; Wang, J.; Yang, Q.; Liu, C.; Huang, D.; Zhu, T. Graphene's Cousin: the Present and Future of Graphane. *Nanoscale Res. Lett.* **2014**, *9*, 26.

(7) Saraswat, V.; Jacobberger, R. M.; Arnold, M. S. Materials Science Challenges to Graphene Nanoribbon Electronics. *ACS Nano* **2021**, *15*, 3674−3708.

(8) Gu, Y.; Qiu, Z.; Müllen, K. Nanographenes and Graphene Nanoribbons as Multitalents of Present and Future Materials Science. *J. Am. Chem. Soc.* **2022**, *144*, 11499−11524.

(9) Chen, Z.; Narita, A.; Müllen, K. Graphene Nanoribbons: On-Surface Synthesis and Integration into Electronic Devices. *Adv. Mater.* **2020**, *32*, 2001893.

(10) Savini, G.; Ferrari, A. C.; Giustino, F. First-Principles Prediction of Doped Graphane as a High-Temperature Electron-Phonon Superconductor. *Phys. Rev. Lett.* **2010**, *105*, No. 037002.

(11) Gharekhanlou, B.; Khorasani, S. Current-Voltage Characteristics of Graphane *p-n* Junctions. *IEEE Trans. Electron Devices* **2010**, *57*, 209−214.

(12) Yan, L.; Zheng, Y.; Zhao, F.; Li, S.; Gao, X.; Xu, B.; Weiss, P. S.; Zhao, Y. Chemistry and Physics of a Single Atomic Layer: Strategies and Challenges for Functionalization of Graphene and Graphene-Based Materials. *Chem. Soc. Rev.* **2012**, *41*, 97−114.

(13) Wen, X.; Hand, L.; Labet, V.; Yang, T.; Hoffmann, R.; Ashcroft, N. W.; Oganov, A. R.; Lyakhov, A. O. Graphane Sheets and Crystals under Pressure. *Proc. Natl. Acad. Sci. U. S. A.* **2011**, *108*, 6833−6837.

(14) Zhou, J.; Wang, Q.; Sun, Q.; Chen, X.; Kawazoe, Y.; Jena, P. Ferromagnetism in Semihydrogenated Graphene Sheet. *Nano Lett.* **2009**, *9*, 3867−3870.

(15) Ji, C.; Adeleke, A. A.; Yang, L.; Wan, B.; Gou, H.; Yao, Y.; Li, B.; Meng, Y.; Smith, J. S.; Prakapenka, V. B.; Liu, W.; Shen, G.; Mao, W. L.; Mao, H.-k. Nitrogen in Black Phosphorus Structure. *Sci. Adv.* **2020**, *6*, No. eaba9206.

(16) Bhattacharya, A.; Bhattacharya, S.; Majumder, C.; Das, G. P. Third Conformer of Graphane: A First-Principles Density Functional Theory Study. *Phys. Rev. B* **2011**, *83*, No. 033404.

(17) Lebègue, S.; Klintenberg, M.; Eriksson, O.; Katsnelson, M. I. Accurate Electronic Band Gap of Pure and Functionalized Graphane from GW Calculations. *Phys. Rev. B* **2009**, *79*, 245117.

(18) Bagusetty, A.; Livingston, J.; Johnson, J. K. Graphamine: Amine-Functionalized Graphane for Intrinsic Anhydrous Proton Conduction. *J. Phys. Chem. C* **2019**, *123*, 1566−1571.

(19) Buonocore, F.; Capasso, A.; Lisi, N. An Ab Initio Study of Hydroxylated Graphene. *J. Chem. Phys.* **2017**, *147*, 104705.

(20) Burgess, J. S.; Matis, B. R.; Robinson, J. T.; Bulat, F. A.; Keith Perkins, F.; Houston, B. H.; Baldwin, J. W. Tuning the Electronic Properties of Graphene by Hydrogenation in a Plasma Enhanced Chemical Vapor Deposition Reactor. *Carbon* **2011**, *49*, 4420−4426.

(21) Poh, H.; Šaněk, F.; Sofer, Z.; Pumera, M. High-Pressure Hydrogenation of Graphene: towards Graphane. *Nanoscale* **2012**, *4*, 7006−7011.

(22) Zhang, X.; Huang, Y.; Chen, S.; Kim, N. Y.; Kim, W.; Schilter, D.; Biswal, M.; Li, B.; Lee, Z.; Ryu, S.; Bielawski, C. W.; Bacsa, W. S.; Ruoff, R. S. Birch-Type Hydrogenation of Few-Layer Graphenes: Products and Mechanistic Implications. *J. Am. Chem. Soc.* **2016**, *138*, 14980−14986.

(23) Whitener, K. E.; Lee, W. K.; Campbell, P. M.; Robinson, J. T.; Sheehan, P. E. Chemical Hydrogenation of Single-Layer Graphene Enables Completely Reversible Removal of Electric Conductivity. *Carbon* **2014**, *72*, 348−353.

(24) Subrahmanyam, K. S.; Kumar, P.; Maitra, U.; Govindaraj, A.; Hembram, K. P. S. S.; Waghmare, U. V.; Rao, C. N. R. Chemical Storage of Hydrogen in Few-Layer Graphene. *Proc. Natl. Acad. Sci. U. S. A.* **2011**, *108*, 2674−2677.

(25) Funnell, N. P.; Dawson, A.; Marshall, W. G.; Parsons, S. Destabilisation of Hydrogen Bonding and the Phase Stability of Aniline at High Pressure. *CrystEngComm* **2013**, *15*, 1047−1060.

(26) Flores, M. Z. S.; Autreto, P. A. S.; Legoas, S. B.; Galvao, D. S. Graphene to Graphane: a Theoretical Study. *Nanotechnology* **2009**, *20*, 465704.

(27) Li, F.; Xu, J.; Wang, Y.; Zheng, H.; Li, K. Pressure-Induced Polymerization: Addition and Condensation Reactions. *Molecules* **2021**, *26*, 7581.

(28) Zhao, W.; Zhang, J.; Sun, Z.; Xiao, G.; Zheng, H.; Li, K.; Li, M.; Zou, B. Chemical Synthesis Driven by High Pressure. *CCS Chem.* **2025**, 1.

(29) Zhang, P.; Tang, X.; Wang, Y.; Wang, X.; Gao, D.; Li, Y.; Zheng, H.; Wang, Y.; Wang, X.; Fu, R.; Tang, M.; Ikeda, K.; Miao, P.; Hattori, T.; Sano-Furukawa, A.; Tulk, C. A.; Molaison, J. J.; Dong, X.;

Li, K.; Ju, J.; Mao, H.-k. Distance-Selected Topochemical Dehydro-Diels-Alder Reaction of 1, 4-Diphenylbutadiyne toward Crystalline Graphitic Nanoribbons. *J. Am. Chem. Soc.* **2020**, *142*, 17662−17669.
(30) Li, Y.; Tang, X.; Zhang, P.; Wang, Y.; Yang, X.; Wang, X.; Li, K.; Wang, Y.; Wu, N.; Tang, M.; Xiang, J.; Lin, X.; Lee, H. H.; Dong, X.; Zheng, H.; Mao, H.-k. Scalable High-Pressure Synthesis of sp^2-sp^3 Carbon Nanoribbon via [4 + 2] Polymerization of 1, 3, 5-Triethynylbenzene. *J. Phys. Chem. Lett.* **2021**, *12*, 7140−7145.
(31) Zhang, P.; Gao, D.; Tang, X.; Yang, X.; Zheng, H.; Wang, Y.; Wang, X.; Xu, J.; Wang, Z.; Liu, J.; Wang, X.; Ju, J.; Tang, M.; Dong, X.; Li, K.; Mao, H.-k. Ordered Van der Waals Hetero-Nanoribbon from Pressure-Induced Topochemical Polymerization of Azobenzene. *J. Am. Chem. Soc.* **2023**, *145*, 6845−6852.
(32) Gao, D.; Tang, X.; Xu, J.; Yang, X.; Zhang, P.; Che, G.; Wang, Y.; Chen, Y.; Gao, X.; Dong, X.; Zheng, H.; Li, K.; Mao, H.-k. Crystalline $C_3N_3H_3$ Tube (3,0) Nanothreads. *Proc. Natl. Acad. Sci. U. S. A.* **2022**, *119*, No. e2201165119.
(33) Wang, X.; Yang, X.; Wang, Y.; Tang, X.; Zheng, H.; Zhang, P.; Gao, D.; Che, G.; Wang, Z.; Guan, A.; Xiang, J.; Tang, M.; Dong, X.; Li, K.; Mao, H.-k. From Biomass to Functional Crystalline Diamond Nanothread: Pressure-Induced Polymerization of 2,5-Furandicarboxylic Acid. *J. Am. Chem. Soc.* **2022**, *144*, 21837−21842.
(34) Huss, S.; Wu, S.; Chen, B.; Wang, T.; Gerthoffer, M. C.; Ryan, D. J.; Smith, S. E.; Crespi, V. H.; Badding, J. V.; Elacqua, E. Scalable Synthesis of Crystalline One-Dimensional Carbon Nanothreads through Modest-Pressure Polymerization of Furan. *ACS Nano* **2021**, *15*, 4134−4143.
(35) Biswas, A.; Ward, M. D.; Wang, T.; Zhu, L.; Huang, H. T.; Badding, J. V.; Crespi, V. H.; Strobel, T. A. Evidence for Orientational Order in Nanothreads Derived from Thiophene. *J. Phys. Chem. Lett.* **2019**, *10*, 7164−7171.
(36) Sun, J.; Dong, X.; Wang, Y.; Li, K.; Zheng, H.; Wang, L.; Cody, G. D.; Tulk, C. A.; Molaison, J. J.; Lin, X.; Meng, Y.; Jin, C.; Mao, H.-k. Pressure-Induced Polymerization of Acetylene: Structure-Directed Stereoselectivity and a Possible Route to Graphane. *Angew. Chem., Int. Ed.* **2017**, *56*, 6553−6557.
(37) Wang, Y.; Dong, X.; Tang, X.; Zheng, H.; Li, K.; Lin, X.; Fang, L.; Sun, G.; Chen, X.; Xie, L.; Bull, C. L.; Funnell, N. P.; Hattori, T.; Sano-Furukawa, A.; Chen, J.; Hensley, D. K.; Cody, G. D.; Ren, Y.; Lee, H. H.; Mao, H.-k. Pressure-Induced Diels-Alder Reactions in C_6H_6-C_6F_6 Cocrystal towards Graphane Structure. *Angew. Chem., Int. Ed.* **2019**, *58*, 1468−1473.
(38) Tang, X.; Dong, X.; Zhang, C.; Li, K.; Zheng, H.; Mao, H.-k. Triggering Dynamics of Acetylene Topochemical Polymerization. *Matter Radiat. Extrem.* **2023**, *8*, No. 058402.
(39) Blake, A. J.; Champness, N. R.; Cooke, P. A.; Nicolson, J. E. B.; Wilson, C. Multi-Modal Bridging Ligands; Effects of Ligand Functionality, Anion and Crystallization Solvent in Silver(I) Coordination Polymers. *J. Chem. Soc., Dalton Trans.* **2000**, 3811−3819.
(40) Chen, B.; Hoffmann, R.; Ashcroft, N. W.; Badding, J. V.; Xu, E.; Crespi, V. H. Linearly Polymerized Benzene Arrays as Intermediates, Tracing Pathways to Carbon Nanothreads. *J. Am. Chem. Soc.* **2015**, *137*, 14373−14386.
(41) Nobrega, M. M.; Teixeira-Neto, E.; Cairns, A. B.; Temperini, M. L. A.; Bini, R. One-Dimensional Diamondoid Polyaniline-Like Nanothreads from Compressed Crystal Aniline. *Chem. Sci.* **2018**, *9*, 254−260.
(42) Talbot, A.; Devarajan, D.; Gustafson, S. J.; Fernandez, I.; Bickelhaupt, F. M.; Ess, D. H. Activation-Strain Analysis Reveals Unexpected Origin of Fast Reactivity in Heteroaromatic Azadiene Inverse-Electron-Demand Diels-Alder Cycloadditions. *J. Org. Chem.* **2015**, *80*, 548−558.
(43) Sengupta, A.; Li, B.; Svatunek, D.; Liu, F.; Houk, K. N. Cycloaddition Reactivities Analyzed by Energy Decomposition Analyses and the Frontier Molecular Orbital Model. *Acc. Chem. Res.* **2022**, *55*, 2467−2479.
(44) Che, G.; Fei, Y.; Tang, X.; Zhao, Z.; Hattori, T.; Abe, J.; Wang, X.; Ju, J.; Dong, X.; Wang, Y.; Li, K.; Zheng, H. Pressure-Induced Polymerization of 1,4-Difluorobenzene towards Fluorinated Diamond Nanothreads. *Phys. Chem. Chem. Phys.* **2025**, *27*, 1112−1118.
(45) Zhao, Z.; Che, G.; Li, F.; Fei, Y.; Luo, H.; Lang, P.; Zeng, Q.; Bai, H.; Wang, Y.; Mao, H.-k.; Zheng, H.; Li, K. Synthesis of a Biphenylene Nanoribbon by Compressing Biphenylene under Extreme Conditions. *Phys. Chem. Chem. Phys.* **2025**, *27*, 6072−6078.
(46) Ciabini, L.; Santoro, M.; Gorelli, F. A.; Bini, R.; Schettino, V.; Raugei, S. Triggering Dynamics of the High-Pressure Benzene Amorphization. *Nat. Mater.* **2007**, *6*, 39−43.
(47) Foy, D.; Demazeau, G.; Florian, P.; Massiot, D.; Labrugère, C.; Goglio, G. Modulation of the Crystallinity of Hydrogenated Nitrogen-rich Graphitic Carbon Nitrides. *J. Solid State Chem.* **2009**, *182*, 165−171.
(48) Lotsch, B. V.; Schnick, W. New Light on an Old Story: Formation of Melam during Thermal Condensation of Melamine. *Chem. Eur. J.* **2007**, *13*, 4956−4968.
(49) Jürgens, B.; Irran, E.; Senker, J.; Kroll, P.; Müller, H.; Schnick, W. Melem (2,5,8-triamino-tri-s-triazine), an Important Intermediate During Condensation of Melamine Rings to Graphitic Carbon Nitride: Synthesis, Structure Determination by X-ray Powder Diffractometry, Solid-State NMR, and Theoretical Studies. *J. Am. Chem. Soc.* **2003**, *125*, 10288−10300.
(50) Pretsch, E.; Bühlmann, P.; Badertscher, M. *Structure Determination of Organic Compounds: Tables of Spectral Data*, 4th ed.; Springer Berlin Heidelberg Press, 2009; pp 118−120.
(51) Demingos, P. G.; Muniz, A. R. Electronic and Mechanical Properties of Partially Saturated Carbon and Carbon Nitride Nanothreads. *J. Phys. Chem. C* **2019**, *123*, 3886−3891.
(52) Luc, N.; Dang, V.; Nguyen, H.; Mai, A. Micro-Rod Single-Crystalline Phthalocyanine for Photodetector Development. *Mater. Sci. Semicond. Process.* **2021**, *125*, 105638.
(53) Cao, Y.; Dou, J.; Zhao, N.; Zhang, S.; Zheng, Y.; Zhang, J.; Wang, J.; Pei, J.; Wang, Y. Highly Efficient NIR-II Photothermal Conversion based on an Organic Conjugated Polymer. *Chem. Mater.* **2017**, *29*, 718−725.
(54) Kawabata, K.; Saito, M.; Osaka, I.; Takimiya, K. Very Small Bandgap π-Conjugated Polymers with Extended Thienoquinoids. *J. Am. Chem. Soc.* **2016**, *138*, 7725−7732.

https://doi.org/10.1021/jacs.5c03116
J. Am. Chem. Soc. 2025, 147, 14054−14059